Multipath Propagation Theory and Modeling in Wideband Mobile Radio: The "ETP Model", Connecting 'Propagation" and "Systems"

Y. Karasawa

Abstract

A very simple, general scheme for calculating the irreducible bit-error rate (BER) – namely, the BER floor – due to inter-symbol interference (ISI) in frequency-selective Nakagami-Rice fading environments has been developed. The scheme, which we call the Equivalent Transmission-Path (ETP) model, makes a general connection between "wave propagation" and "digital transmission characteristics." In this paper we present a consistent calculation formula for the BER due to ISI, by re-examining the information in our previous papers on the ETP model. Moreover, we demonstrate an application of the ETP model to the indoor propagation environment.

1. Introduction

Modeling of Nakagami-Rice fading, or so-called Ricean fading, is expected to play an important role in the design of wideband and high-capacity mobile systems. Examples include indoor wireless communication systems, short-range wireless access systems, and mobile satellite systems (MSS), which can enrich personal communications. The model of Nakagami-Rice fading, which appears in line-of-sight radio communications environments, is more general than that of Rayleigh fading. In fact, Rayleigh fading is a special case of Nakagami-Rice fading. The propagation environments are shown in Figure 1.

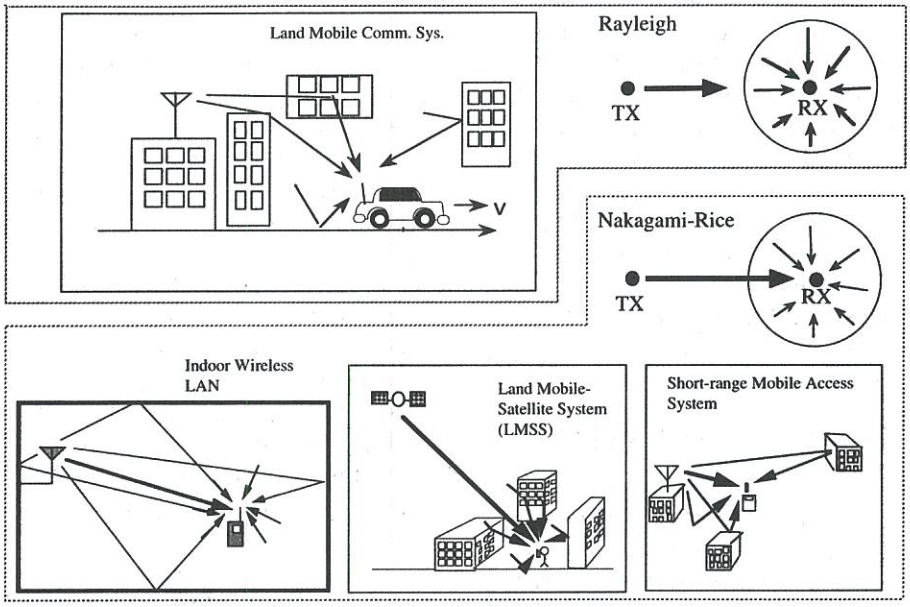

Figure 1. Multipath fading environments (Rayleigh fading and Nakagami-Rice fading).

Prof. Yoshio Karasawa is with
The University of Electro-Communications
1-5-1 Chofugaoka, Chofu-shi,
Tokyo 182-8585, Japan
Tel: +81 424-43-5172
Fax: +81 424-43-5210
E-mail: karasawa@ee.uec.ac.jp

[Editor's note: This paper is invited.]

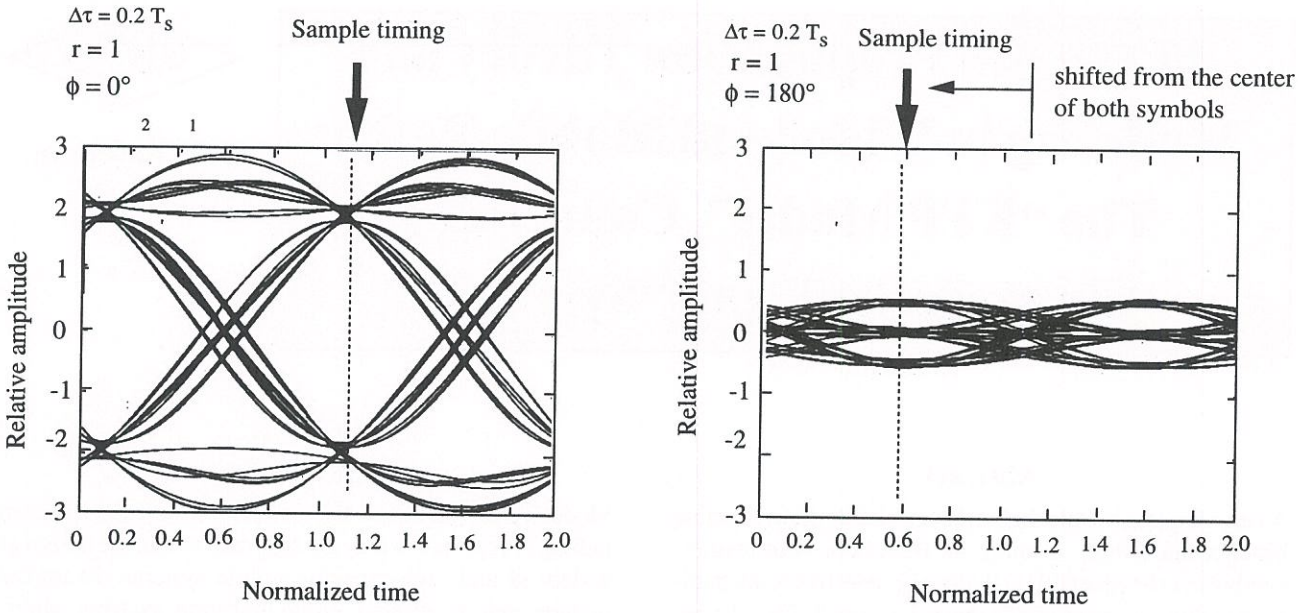

Figure 2. The eye patterns of the received signal for $r=1$ and $\Delta\tau=0.2T_s$: (a) $\phi=0°$; (b) $\phi=180°$.

Based on a series of numerical analyses using computer simulations and theoretical considerations, we have proposed a simplified propagation model for assessing wideband digital transmission characteristics in frequency-selective Nakagami-Rice fading environments [1-4]. We have called this the Equivalent Transmission-Path (ETP) model. Moreover, we have used this model to derive a straightforward calculation formula for error-occurrence characteristics due to inter-symbol interference (ISI) in frequency-selective Nakagami-Rice fading environments.

In this tutorial paper, a consistent calculation formula for predicting the BER due to ISI is presented, by reconfiguring our papers published so far on the ETP model from a practical viewpoint. In addition, an application of this model to indoor propagation is demonstrated.

2. Occurrence of Bit Errors due to ISI

Before introducing the ETP model, let us review the occurrence of bit errors due to inter-symbol interference (ISI), under the frequency-selective fading condition [5]. The following time-invariant two-wave condition, which is the simplest case producing frequency-selective fading, is considered first.

$$h(\tau)=a_1\delta(\tau)+a_2\overset{\delta}{\wedge}(\tau-\Delta\tau) \qquad (1a)$$

$$=a_1\left[\delta(\tau)+re^{j\phi}\delta(\tau-\Delta\tau)\right], \qquad (1b)$$

where h is the impulse response, τ is the delay, a_i ($i=1,2$) is the complex envelope of the ith wave, δ is the delta function, and $\Delta\tau$ is the delay difference between the preceding wave and the delayed wave. In Equation (1b), r is the amplitude ratio, defined as $|a_2/a_1|$, and ϕ is the phase difference between the two waves. Throughout this paper, our main concern is for $\Delta\tau$ within the range of the symbol-duration time, T_s, namely, $\Delta\tau<T_s$. When dealing with errors due to ISI, the parameters r and ϕ are more essential than a_1 and a_2, because irreducible errors due to ISI become independent of the amplitude of each wave.

Figure 2 shows the eye pattern of the received signal for $r=1$ and $\Delta\tau=0.2T_s$, for $\phi=0°$ and $\phi=180°$. We can easily understand that only the case of Figure 2b causes errors due to ISI. This means that the error-occurrence condition depends not only on $\Delta\tau$, but also on r and ϕ. This raises the question, "What is the condition where the error occurs?" The answer is given in Figure 3. This figure shows that the error-occurrence area for CQPSK (quadrature phase shift keying with coherent detection) is a function of r and ϕ while $\Delta\tau=0.2T_s$. Different patterns can be seen for each modulation/demodulation scheme. We call this figure a BER map.

3. Basic Expression for Multipath Environments

It is assumed that the time-variation speed of the channel is sufficiently slower than the data-transmission speed. In other words, the multipath-fading environment remains constant during the data-symbol period. Under this condition, an instantaneous multipath environment at a given position and at a given time, t, can be expressed in terms of the slowly time-varying impulse response [6, 7]. This is given by

$$h(\tau,t)=\sum_{i=0}^{\infty}a_i(t)\delta\left[\tau-\tau_i(t)\right] \qquad (2)$$

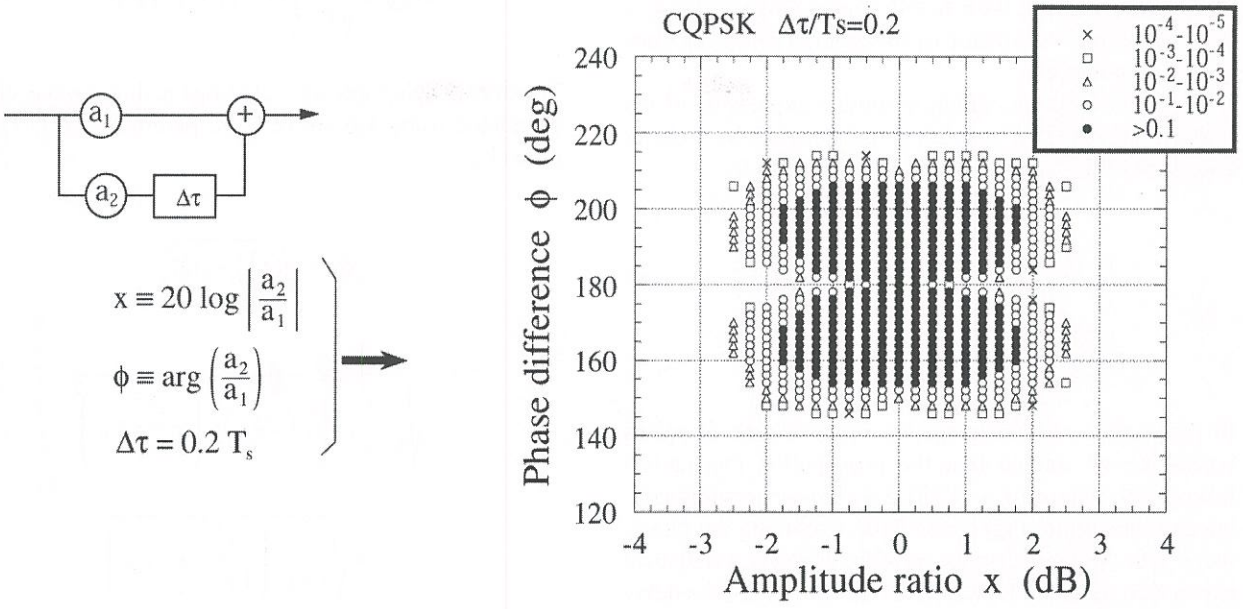

Figure 3. The error-occurrence area for $\Delta\tau = 0.2T_s$ in CQPSK (hereafter, we call this a BER map).

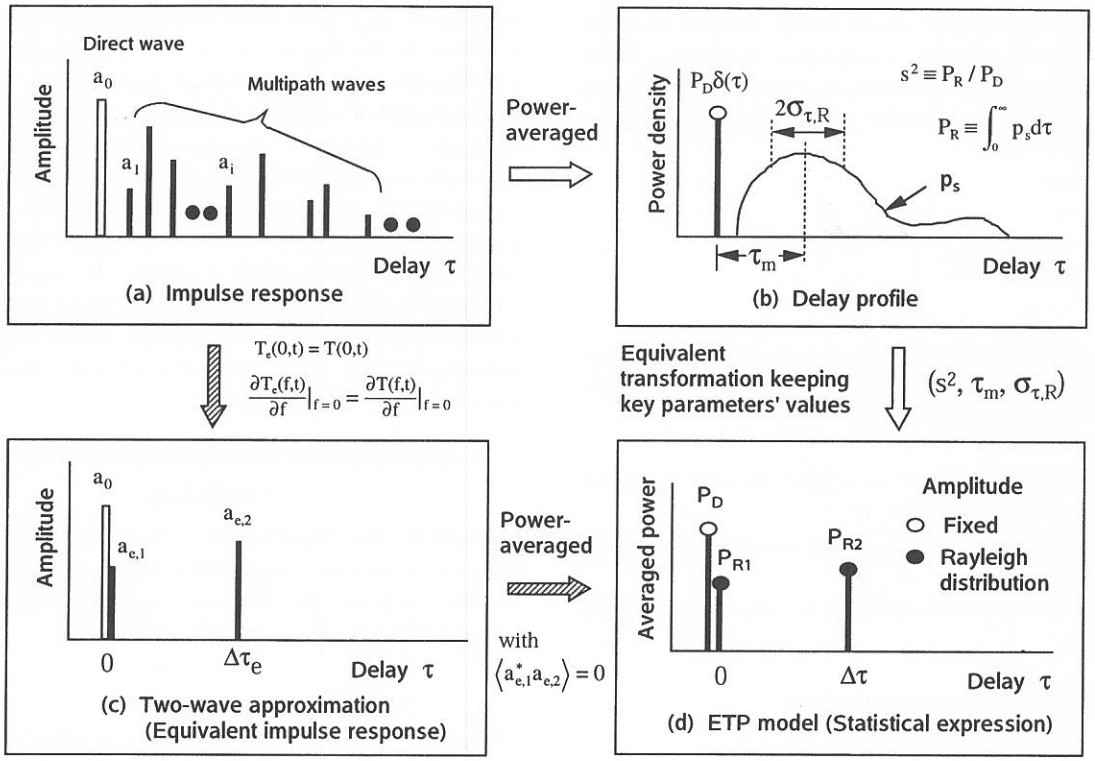

Figure 4. Various expressions of the Nakagami-Rice fading environment (instantaneous versus statistical).

where a_i is the complex amplitude of the ith incident wave in the multipath waves. For modeling, we assign the direct wave path to be $i=0$ with $\tau_0=0$. The impulse response is shown in Figure 4a. For the case of Rayleigh fading, a_0 must be 0 when modeling.

The transfer function, which is another expression of the instantaneous fading condition, is obtained by Fourier transform of the impulse response. It is given by

$$T(f,t)=\int_0^\infty h(\tau,t)\exp(-j2\pi f\tau)d\tau \qquad (3)$$
$$=\sum_{i=0}^{\infty}a_i(t)\exp\left[-j2\pi f\tau_i(t)\right]$$

In the mobile radio-propagation environment, it seems acceptable to assume that the propagation mechanism follows the nature of a WSSUS (wide-sense stationary, uncorrelated scattering) channel [6], excluding the direct-wave path. The power-delay profile, which is a statistical expression of the multipath environment in the time-delay domain, is given by

$$p(\tau)=\left\langle h^*(\tau,t)h(\tau,t)\right\rangle \qquad (4)$$
$$=P_D\delta(\tau-\tau_0)+p_s(\tau)$$

where $\langle\circ\rangle$ means the ensemble average (or the time-domain average, if the process is ergodic), P_D is the direct wave power, and p_s is the averaged power density of multipath waves. The delay profile given in Equation (4) is an idealized profile, from the viewpoint of propagation modeling, while a measurable profile is a continuous function, due to the averaging effect of a receiver filter. The total multipath power is given by

$$P_R=\int_0^\infty p_s(\tau)d\tau\cdot \qquad (5)$$

Figure 4b shows a delay profile for Nakagami-Rice fading. In this figure, the following three key parameters (which will be explained in a later section) are given:

1. s^2: The ratio of the mean multipath power (P_R) to the direct wave power (P_D) [$=P_R/P_D$].
2. τ_m: The mean delay of multipath waves relative to the delay of the direct wave.
3. $\sigma_{\tau,R}$: The delay spread of multipath waves (excluding the direct wave)

τ_m and $\sigma_{\tau,R}$ are given respectively by

$$\tau_m=\frac{1}{P_R}\int_0^\infty \tau p_s(\tau)d\tau \qquad (6)$$

$$\sigma_{\tau,R}=\sqrt{\frac{1}{P_R}\int_0^\infty(\tau-\tau_m)^2p_s(\tau)d\tau} \qquad (7)$$

The overall delay spread, including the direct wave, can be calculated using the above three parameters [1]. This is given by

$$\sigma_\tau=\sqrt{\left\langle\tau^2\right\rangle-\left\langle\tau\right\rangle^2}$$

$$=\sqrt{\frac{s^2}{1+s^2}\left(\tau_m^2+\sigma_{\tau,R}^2\right)-\left(\frac{s^2}{1+s^2}\tau_m\right)^2}$$

$$=\sqrt{\frac{s^2}{1+s^2}\left(\frac{\tau_m^2}{1+s^2}+\sigma_{\tau,R}^2\right)} \qquad (8)$$

In order to show an example, let us analyze the wideband digital transmission characteristics in indoor environments for a wireless LAN. Figure 5a shows the multipath profile of a rectangular-type indoor environment, where the transmitter (TX) point and the receiver (RX) point are, respectively, set at (x, y, z) coordinates of (2, 8, 2) and (13, 2, 1), in a room of (15, 10, 3) meters. The three-dimensional path profile was obtained by a ray-tracing scheme based on the image method [8-12]. Figure 5b shows the impulse response with a reflection coefficient, γ, of 0.7 (a probable value for plasterboard with attached rock wool, in the case of an oblique angle of incidence [13]) for every wall. Figures 6a-6c show examples of the spatial distribution of error occurrence for CQPSK with data-transmission bit rates of 2, 5, and 10 Mbps, at a frequency of 5 GHz [12]. In the figure, points where the BER exceeds 10^{-1} are marked by large dots, and points where the BER exceeds 10^{-3} are marked by smaller dots. The data shown in Figures 6a-6c were obtained by computer simulation, based on ray tracing and CQPSK data transmission. The data shown in Figures 6d-6f will be mentioned in a later section.

4. Equivalent Transformation of Impulse Response

To maintain the characteristics of frequency selectivity, at least two waves are necessary, as shown in Figure 4c. The impulse response and frequency transfer function of the two-wave model are given, respectively, by

$$h_c(\tau,t)=\left[a_0+a_{c,1}(t)\right]\delta(\tau)+a_{c,2}(t)\delta(\tau-\Delta\tau_c) \qquad (9)$$

$$T_c(f,t)=a_0+a_{c,1}(t)+a_{c,2}(t)\exp(-j2\pi f\Delta\tau_c) \qquad (10)$$

In order to keep the equivalence for assessing digital-transmission characteristics, we can connect the two transfer functions by the following conditions [2]:

$$T_e(0,t) = T(0,t) \tag{11}$$

$$\left.\frac{\partial T_e(f,t)}{\partial f}\right|_{f=0} = \left.\frac{\partial T(f,t)}{\partial f}\right|_{f=0} \tag{12}$$

By the above equations, the path amplitude and its frequency dependence at $f = 0$ (namely, at the carrier frequency for the RF signal) are set to be equal to each other. These conditions lead to

$$a_{e,1}(t) = \sum_{i=1}^{\infty} a_i(t) - \frac{\sum_{i=1}^{\infty} a_i(t)\tau_i(t)}{\Delta\tau_e} \tag{13}$$

$$a_{e,2}(t) = \frac{\sum_{i=1}^{\infty} a_i(t)\tau_i(t)}{\Delta\tau_e} \tag{14}$$

No strict condition is imposed to determine the value of $\Delta\tau_e$, if the following condition is satisfied. From our examination by computer simulations [1, 12], and as will be seen in Figure 8, the condition for the application of this method is as follows:

$$\tau_m \le 0.3T_s \text{ and } \sigma_{\tau,R} \le 0.3T_s \tag{15}$$

For the ray-tracing case, the mean delay, τ_m, and the delay spread of multipath waves, $\sigma_{\tau,R}$, can be roughly estimated by

$$\tau_m \approx \frac{\sum_{i=1}^{\infty} \tau_i |a_i|^2}{\sum_{i=1}^{\infty} |a_i|^2} \tag{16}$$

$$\sigma_{\tau,R} \approx \sqrt{\frac{\sum_{i=1}^{\infty} (\tau_i - \tau_m)^2 |a_i|^2}{\sum_{i=1}^{\infty} |a_i|^2}} \tag{17}$$

Under this condition, the BER, P_e, can be estimated from the BER map of $\Delta\tau_{map}$, E, by

$$P_e = E(r, \phi; \Delta\tau_e), \tag{18}$$

where

$$r = \left|a_{e,2}/(a_0 + a_{e,1})\right|, \phi = \arg\left[a_{e,2}/(a_0 + a_{e,1})\right] \tag{19}$$

$$\Delta\tau_e = \Delta\tau_{map}. \tag{20}$$

Although any kind of BER map, ranging from $\Delta\tau_{map} = 0.1T_s$ to $0.6T_s$, gives almost the same estimate of BER due to ISI, the use of $\Delta\tau_{map} = 0.2T_s$ (which is shown in Figure 3) is suggested [12].

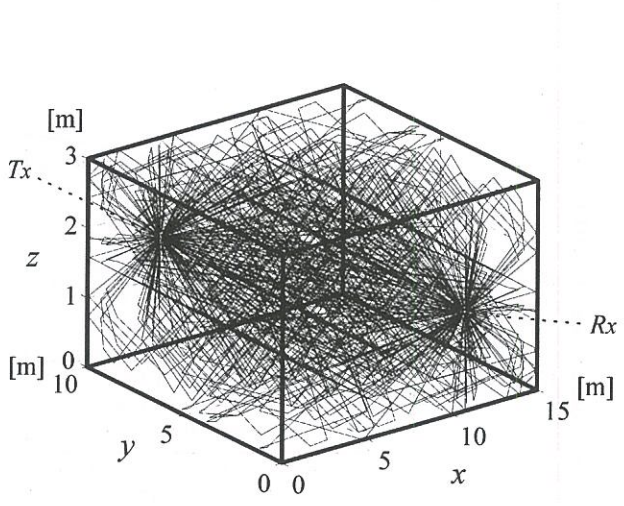

(a) Ray-tracing profile

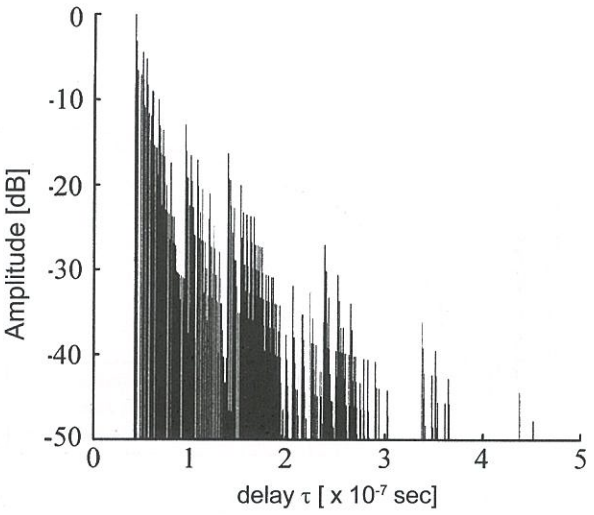

(b) Impulse response

Figure 5. The indoor propagation environment: (a) A ray-tracing profile; (b) The impulse response.

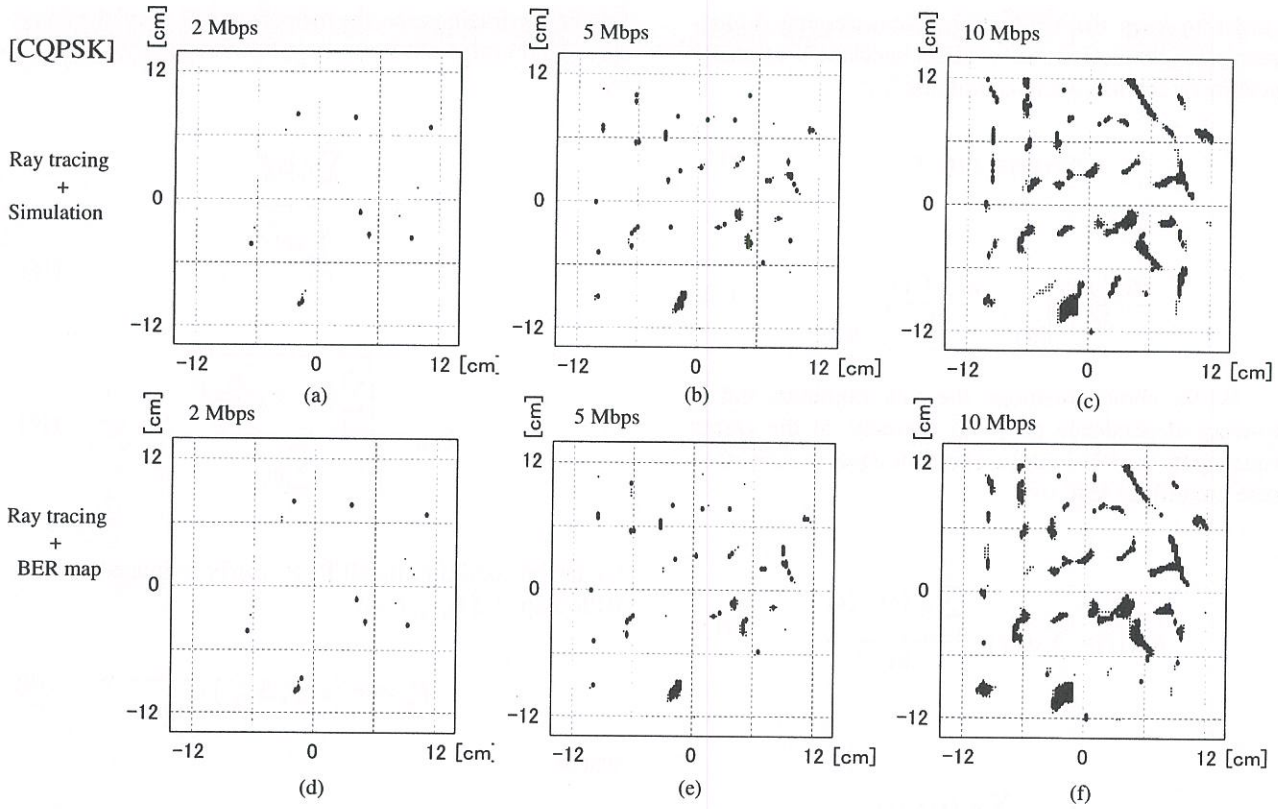

Figure 6. A spatial map of error occurrence for CQPSK with data rates of 2, 5, and 10 Mbps. The upper maps are for the Ray tracing + digital transmission simulation method, while the lower maps are for the Ray tracing + BER method. Points where the BER exceeds 10^{-1} are marked by large dots, and points where the BER exceeds 10^{-3} are marked by smaller dots.

Figures 6d-6f show the spatial distribution of error occurrence for CQPSK, calculated using the above method, namely, (1) obtaining the impulse response by means of ray tracing (see Figure 5); and (2) calculating the BER from Equations (18) and (19), with a BER map, E. We call this method "Ray tracing + BER map." Figures 6d-6f, respectively, correspond to the cases of Figures 6a-6c, calculated based on (1) ray tracing, and (2) rigorous digital-transmission simulation in the multipath environment determined by the ray tracing. We call this method "Ray tracing + Simulation." The averaged BER and the location percentage of error occurrence – namely, the error-occurrence rate (EOR) in the four-wavelength-square area (24 cm × 24 cm) for CQPSK – are compared in Figure 7 (the black dots and the white dots). As seen in Figures 6 and 7, the results of our proposed scheme agree extremely well with the computer simulation. The

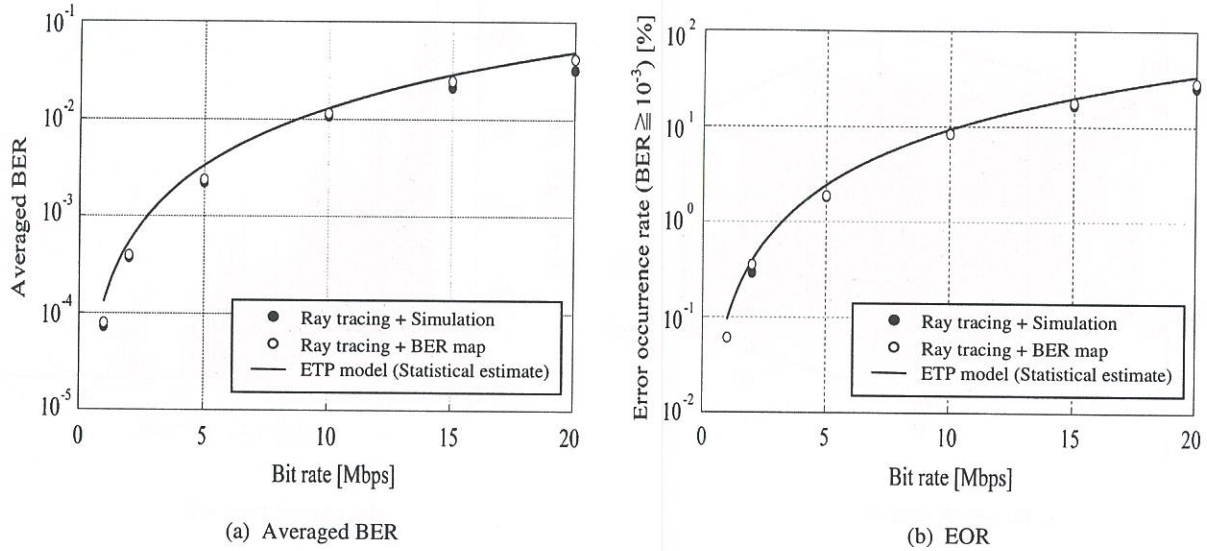

Figure 7. A comparison of the averaged BER (a) and the EOR (b) for three methods. Results given by the ETP model (a statistical simulation), discussed later in the text, are also shown.

computational time to draw one map, shown in Figures 6a, 6b, or 6c, was more than five hours on a personal computer, excluding the common part of the ray tracing, while the proposed method took only three minutes. The calculation speed of the proposed method is 100 times faster. In Figure 7, a statistical estimate using the ETP model is shown by solid curves. This will be discussed later.

5. Equivalent Transformation of Delay Profile: ETP Model

Next, we will develop a statistical two-wave model for the prediction of the statistical properties of digital-transmission characteristics, namely, the averaged BER under a time-varying multipath fading condition. As stated above, for the approximation of an impulse response, the value of $\Delta\tau_e$ can be set to $\Delta\tau_e = \Delta\tau_{map}$. For statistical modeling in terms of a delay profile, on the other hand, it seems better to select the value of $\Delta\tau_e$ to be where the fluctuations between $a_{e,1}$ and $a_{e,2}$ become independent. By adopting this condition, the modeling is drastically easier. Here, let us determine the value of $\Delta\tau_e$. Using Equations (13) and (14), the correlation coefficient is given by [2]

$$\rho_a = \left\langle a_{c,1}^* a_{c,2} \right\rangle \Big/ \sqrt{\left\langle a_{c,1}^* a_{c,1} \right\rangle \left\langle a_{c,2}^* a_{c,2} \right\rangle}$$

$$= \frac{\tau_m \Delta\tau_c - \tau_m^2 - \sigma_{\tau,R}^2}{\sqrt{\left(\Delta\tau_c^2 - 2\tau_m\Delta\tau_c + \tau_m^2 + \sigma_{\tau,R}^2\right)\left(\tau_m^2 + \sigma_{\tau,R}^2\right)}} \qquad (21)$$

Independence of $a_{e,1}$ and $a_{e,2}$ requires the correlation coefficient to be zero; therefore, in Equation (21), we must impose the following relation:

$$\Delta\tau_e\big|_{\rho_a=0} \equiv \Delta\tau = \left(\tau_m^2 + \sigma_{\tau,R}^2\right)\Big/\tau_m \qquad (22)$$

where $\Delta\tau$ is the value of $\Delta\tau_e$ corresponding to $\rho_a = 0$. In this condition, the mean powers of $a_{e,1}$ and $a_{e,2}$, are respectively given by [2]

$$P_{R1} = \left\langle a_{e,1}^* a_{e,1} \right\rangle\Big|_{\rho_a=0} = \frac{s^2\sigma_{\tau,R}^2}{\tau_m^2 + \sigma_{\tau,R}^2} P_D \qquad (23)$$

$$P_{R2} = \left\langle a_{e,2}^* a_{e,2} \right\rangle\Big|_{\rho_a=0} = \frac{s^2\tau_m^2}{\tau_m^2 + \sigma_{\tau,R}^2} P_D \qquad (24)$$

The statistical two-wave environment determined by Equations (22)-(24) can also be designated by the fading parameters corresponding to s^2, τ_m, and $\sigma_{\tau,R}$. If we let the parameters be s_e^2, $\tau_{m,e}$, and $\sigma_{\tau,R,e}$, then they are given by

$$s_e^2 = \frac{P_{R1} + P_{R2}}{P_D} = s^2 \qquad (25)$$

$$\tau_{m,e} = \frac{P_{R2}\Delta\tau}{P_{R1} + P_{R2}} = \tau_m \qquad (26)$$

$$\sigma_{\tau,R,e} = \frac{\sqrt{P_{R1}P_{R2}}}{P_{R1} + P_{R2}}\Delta\tau = \sigma_{\tau,R} \qquad (27)$$

In Figure 4d, the statistical two-wave model is characterized by the equivalent transformation of the delay profile, maintaining the values of the three fading parameters: s^2, τ_m, and $\sigma_{\tau,R}$. We call these three fading parameters "the key parameters," and the statistical two-wave model is "the equivalent transmission-path (ETP) model."

The relationship of model expressions for the Nakagami-Rice fading environment, in terms of "instantaneous versus statistical" and "multipath versus two-wave approximated," is summarized in Figure 4.

In the statistical two-wave model, which is the ETP model, the preceding wave consists of a constant-wave (namely, the direct wave) component and a Rayleigh-wave component, while the delayed wave is a Rayleigh-wave component. Consequently, the probability density function (PDF) of the amplitude of the preceding wave follows a Nakagami-Rice distribution, and the PDF of the delayed wave follows a

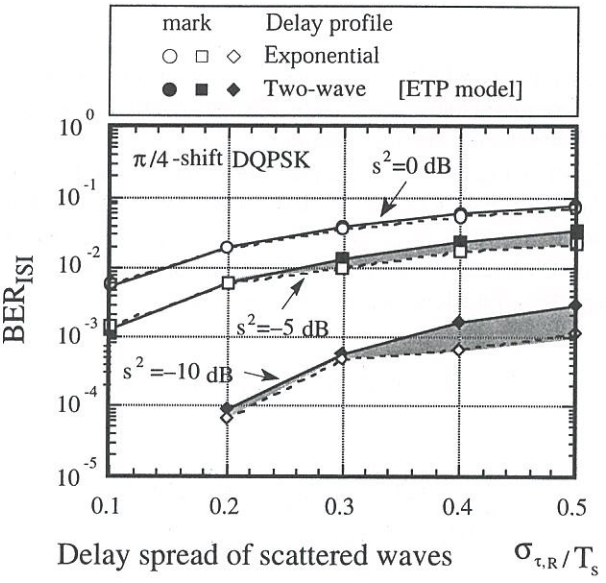

Figure 8. A comparison of the BER due to ISI for two different delay profiles, for the identification of the applicable range of delay spread.

Rayleigh distribution. They are given, respectively, by

$$f_1(r_1;m,\sigma_1)=\frac{r_1}{\sigma_1^2}\exp\left(-\frac{m^2+r_1^2}{2\sigma_1^2}\right)\mathrm{I}_0\left(\frac{mr_1}{\sigma_1^2}\right) \quad (28)$$

$$f_2(r_2;\sigma_2)=\frac{r_2}{\sigma_2^2}\exp\left(-\frac{r_2^2}{2\sigma_2^2}\right) \quad (29)$$

where I_0 is the modified Bessel function of order zero, and the parameters m, σ_1, and σ_2 have the following relationship:

$$P_D=m^2;\quad P_{R1}=2\sigma_1^2;\quad P_{R2}=2\sigma_2^2. \quad (30)$$

Since we chose $\Delta\tau$ so as to be independent for fluctuations of the two Rayleigh waves, the joint PDF for r and ϕ is given by [1]

$$f_{r\phi}(r,\phi;m,\sigma_1,\sigma_2;\Delta\tau)=\frac{\sigma_1^2\sigma_2^2 r}{\pi\left(\sigma_1^2r^2+\sigma_2^2\right)^2}\exp\left(-\frac{m^2}{2\sigma_1^2}\right)F\left[2,1;\frac{m^2\sigma_2^2}{2\sigma_1^2\left(\sigma_1^2r^2+\sigma_2^2\right)}\right]$$

$$=\frac{1}{2\pi}\int_0^\infty f_1(z)\,f_2(zr)\,z\,dz \quad (31)$$

where $F(\alpha,\gamma;z)$ is the confluent hypergeometric function (or Kummer function), for which $\alpha=2$ and $\gamma=1$, given by

$$F(\alpha,\gamma;z)\Big|_{\substack{\alpha=2\\ \gamma=1}}=\sum_{n=0}^{\infty}\frac{(n+1)z^n}{n!} \quad (32)$$

Although the PDF must be given as a function of r and ϕ, the formula actually does not include the variable ϕ, because ϕ follows a uniform distribution.

By replacing the two-wave parameters, m, σ_1, and σ_2 (or P_D, P_{R1}, and P_{R2}) in Equation (31) by the three key parameters, s^2, τ_m, and $\sigma_{\tau,R}$, using the relations in Equations (22)-(27), the joint PDF can be expressed as a function of the key parameters. The PDF is

$$f_{r\phi}\left(r;s^2,\tau_m,\sigma_{\tau,R};\Delta\tau\right)$$

$$=\frac{1}{\pi}\frac{\sigma_{\tau,R}^2\tau_m^2 r}{\left(\sigma_{\tau,R}^2r^2+\tau_m^2\right)^2}\exp\left(-\frac{\tau_m^2+\sigma_{\tau,R}^2}{s^2\sigma_{\tau,R}^2}\right)$$

$$F\left[2,1:\frac{\tau_m^2\left(\tau_m^2+\sigma_{\tau,R}^2\right)}{s^2\sigma_{\tau,R}^2\left(\sigma_{\tau,R}^2r^2+\tau_m^2\right)}\right] \quad (33)$$

In the case of Rayleigh fading (namely, $s^2\gg1$), the formula is simplified to

$$f_{r\phi}(r;\infty,\tau_m,\sigma_\tau;\Delta\tau)=\frac{1}{\pi}\frac{\sigma_\tau^2\tau_m^2 r}{\left(\sigma_\tau^2r^2+\tau_m^2\right)^2} \quad (34a)$$

$$=\frac{1}{\pi}\frac{r}{\left(r^2+1\right)^2}\ \text{(when setting } \tau_m=\sigma_{\tau,R}\text{)}. \quad (34b)$$

Now we are ready to formulate the prediction of BER due to ISI in Rayleigh and Nakagami-Rice fading environments.

6. Formulation of BER due to ISI

The averaged BER due to ISI under a frequency-selective fading condition can be calculated by the following basic equation [1]:

$$BER_{ISI}\left(s^2,\tau_m,\sigma_{\tau,R}\right)$$

$$=\int_0^\infty\int_0^{2\pi} f_{r\phi}\left(r;s^2,\tau_m,\sigma_{\tau,R};\Delta\tau\right)E(r,\phi;\Delta\tau)\,d\phi\,dr \quad (35)$$

where $\Delta\tau$ is given in Equation (22), and E is the specific BER floor of the two-wave model – namely, the BER map – as a function of r and ϕ with a parameter of $\Delta\tau$. Since, as seen in Figure 3, every map is logarithmically symmetrical for $r=1$ (that is, the same value of BER is obtained at $r=r_0$ and $r=1/r_0$), it seems more convenient to use the logarithmic variable in dB, $x\,(=20\log r)$, rather than r, itself. The PDF, $f_{x\phi}(x)$, converted from $f_{r\phi}(r)$, is given by

$$f_{x\phi}(x)=\frac{1}{b}\exp\left(\frac{x}{b}\right)f_{r\phi}\left[\exp\left(\frac{x}{b}\right)\right],\quad\left[b\equiv20\log_{10}(e)\right] \quad (36)$$

By using the above formula, the BER due to ISI, corresponding to Equation (35), can be rewritten with a simplified summation formula as follows:

$$BER_{ISI}\left(s^2,\tau_m,\sigma_{\tau,R}\right)$$

$$=\Delta x\Delta\phi\sum_x\left[f_{x\phi}(x)\sum_\phi E(x,\phi)\right] \quad (37)$$

where Δx (in dB) and $\Delta\phi$ (in radians) are the step sizes of the BER map in x and ϕ such that the calculated values converge sufficiently. Testing showed that a Δx of 0.25 dB and a $\Delta\phi$ of $2\pi/180$ rad (which corresponds to two degrees) are sufficient for QPSK and 16QAM (quadrature amplitude modulation) with $\Delta\tau > 0.1T_s$, while other cases, such as BPSK (binary phase shift keying) or QPSK with $\Delta\tau < 0.1T_s$ need finer step sizes.

Furthermore, to pursue more convenient use, a calculation scheme using only one BER map for each modulation/demodulation scheme is available. To realize this, we utilize the similarity of the BER pattern on the BER map for different $\Delta\tau$ values that are smaller than $0.6T_s$. The following formula can be obtained without loosing prediction accuracy [3]:

$$BER_{ISI}\left(s^2,\tau_m,\sigma_{\tau,R}\right) = \eta^2\Delta x\Delta\phi\sum_x\left[f_{x\phi}(\eta x)\sum_\phi E(x,\phi)\right] \quad (38)$$

with a scaling factor, η, of

$$\eta = \frac{\sigma_{\tau,R}^2+\tau_m^2}{\tau_m}\frac{1}{\Delta\tau_{map}} \quad (39)$$

For the Rayleigh-fading environment, when using Equation (34b) for $f_{r\phi}$, the scaling factor is given by

$$\eta = 2\sigma_\tau/\Delta\tau_{map}. \quad (40)$$

The use of $\Delta\tau_{map} = 0.2T_s$ is suggested, although noticeable differences are not detected when using a map with a $\Delta\tau_{map}$ of less than about $0.4T_s$ [3].

When the effect of thermal noise is not negligible, the following approximation can be made [3]:

$$BER\left(s^2,\tau_m,\sigma_{\tau,R},E_b/N_0\right) = BER_{ISI}\left(s^2,\tau_m,\sigma_{\tau,R}\right)+BER_{TN}\left(E_b/N_0\right) \quad (41)$$

where BER_{TN} is the BER due to thermal noise, and E_b/N_0 is a signal-to-noise ratio parameter, defined by the power for one-bit transmission divided by the noise power density.

For systems where each user terminal moves fast, the long-term-averaged BER in a time domain seems to be a reasonable measure for digital-transmission quality assessment. On the other hand, for systems where the user terminal is at a fixed position, such as in a wireless LAN, the percentage of locations where outage (namely, unacceptable error rate) occurs seems to be a more practical measure, instead of the averaged BER. Throughout this paper, we have called the measure the EOR (error occurrence rate). In this case, the "error occurrence" means that the signal quality specified by the BER comes down to the predetermined threshold value.

The EOR can be calculated by replacing E with P in Equation (38):

$$EOR_{ISI}\left(s^2,\tau_m,\sigma_{\tau,R}\right) = \eta^2\Delta x\Delta\phi\sum_x\left[f_{x\phi}(\eta x)\sum_\phi P(x,\phi)\right] \quad (42)$$

with

$$P(x,\phi) = \begin{cases} 1 \text{ for } E(x,\phi)\geq E_0 \\ 0 \text{ for } E(x,\phi)\leq E_0 \end{cases} \quad (43)$$

where E_0 is the threshold BER for the error occurrence, such as 10^{-3}.

7. Prediction Accuracy and Applicable Parameter Range

To identify the applicable range of parameter values, we performed a computer simulation to compare the results for the two different delay profiles. One is the two-wave model, corresponding to the ETP model, and the other is the exponential delay-profile model. Figure 8 shows the results of comparison. From the figure, the ETP model has high prediction accuracy for multipath environments where τ_m and $\sigma_{\tau,R}$ are less than $0.3T_s$, and when s^2 is above 0 dB ($=1$) – that is, near the Rayleigh fading environment – this limit extends to $0.5T_s$. This is one reason why we restrict the application limit by Equation (15). Within this range, we evaluated the dependence of BER_{ISI} on the delay-profile shape, by assuming the various types of delay profile shown in Figure 9. In this figure, numbers such as "1," "2," and "4" at the top of each impulse state the relative averaged power. The absolute averaged power and the delay (τ_A, τ_B,...), which represent the fading environments, are given in the table in Figure 9. For comparison, eight cases, each of which had eight profiles, were considered. Figure 10 shows the results of the comparison. As can be seen from this figure, there seemed to be no profile dependence on BER_{ISI} when the set of key parameter values was the same. Moreover, the theoretical estimates based on the ETP model, drawn with dotted lines, corresponded fairly well with the results of the simulation. Figure 11 compares the "calculated" versus the

Eight sets of key parameters' values

Case	s^2	τ_m/T_s	$\sigma_{\tau,R}/T_s$	Symbol
1	∞	–	0.1	○
2	∞	–	0.2	●
3	2.0	0.1	0.1	□
4	2.0	0.2	0.2	■
5	1.0	0.1	0.1	△
6	1.0	0.2	0.2	▲
7	0.5	0.1	0.1	◇
8	0.5	0.2	0.2	◆

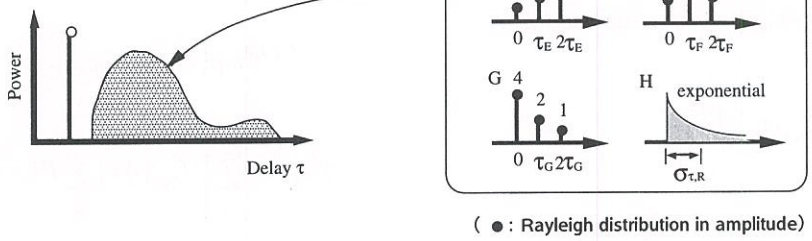

Eight types of delay profiles excluding the direct wave

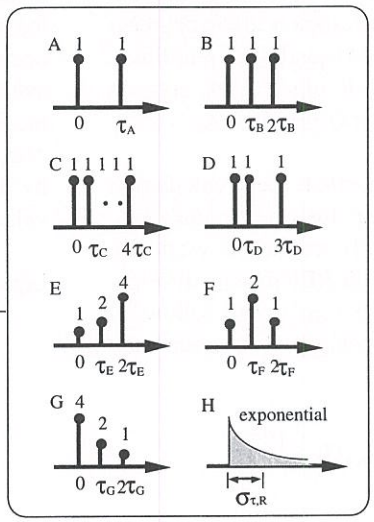

(● : Rayleigh distribution in amplitude)

Figure 9. The delay profiles of scattered waves for the simulation. In the simulation, a constant wave was added to each profile (see lower left) at the place that satisfied the set parameter values in the table (upper left).

"simulated" BER_{ISI} for the various environments given in Figure 9 for CBPSK, CQPSK, and $\pi/4$-DQPSK ($\pi/4$-shift QPSK with differential detection). Figure 7 also shows statistical estimates, drawn with solid curves, corresponding to the cases mentioned in the previous section (namely, the "Ray tracing + Simulation" and "Ray tracing + BER map"). From these figures, we can see an excellent correspondence between the statistical and simulated results for various kinds of fading environments and modulation schemes.

Moreover, as for BER due to ISI and thermal noise mixed concurrently, values calculated by Equation (38) correspond well with simulated values, which are given in Figure 12.

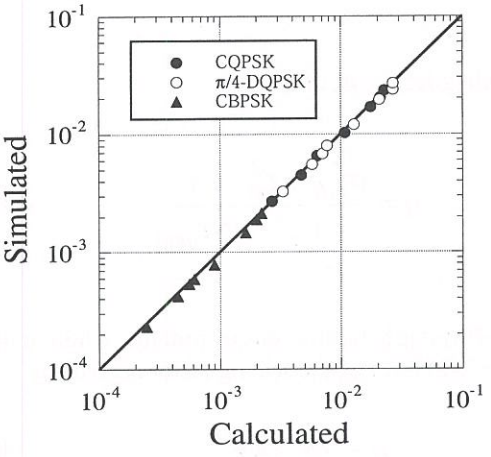

Figure 11. A comparison between a simulated BER floor and a calculated BER floor, based on the ETP model, for various modulation systems.

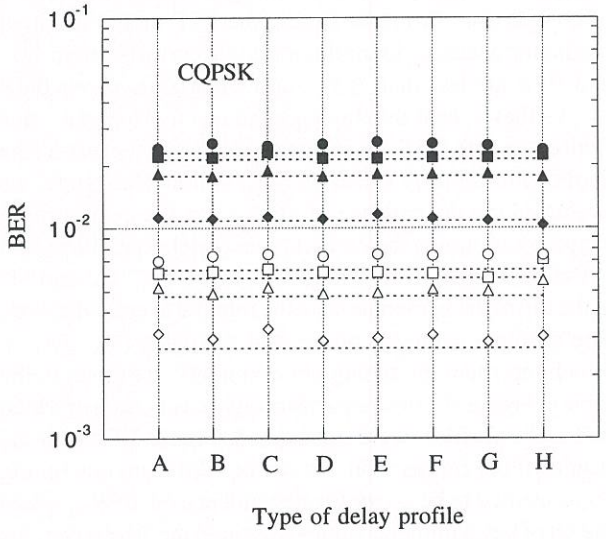

Figure 10. The dependence of the BER on the delay-profile shape. Each mark corresponds to that in the table in Figure 9. The dotted lines are theoretical estimates based on the ETP model, discussed later in the text.

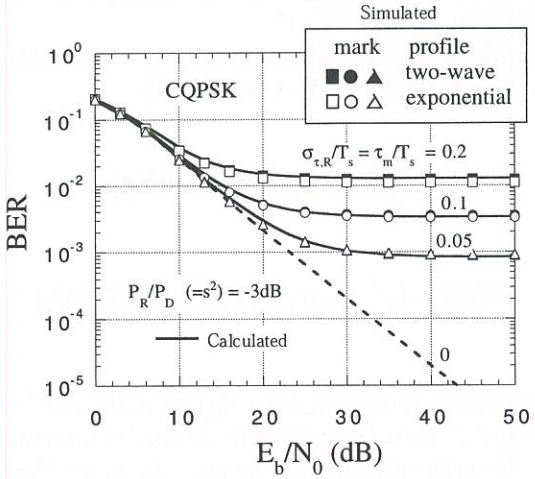

Figure 12. Overall estimates of the BER floor coexisting with thermal noise.

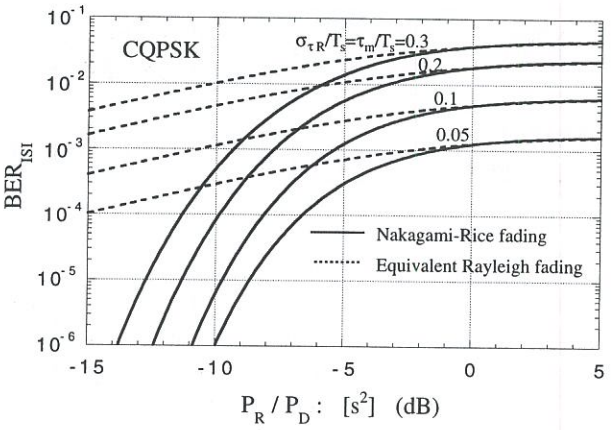

Figure 13. The BER floor characteristics of CQPSK as a function of $s^2\,(P_R/P_D)$ for $\sigma_{\tau,R}/T_s=\tau_m/T_s=0.05$ to 0.3, based on the ETP model (solid lines).

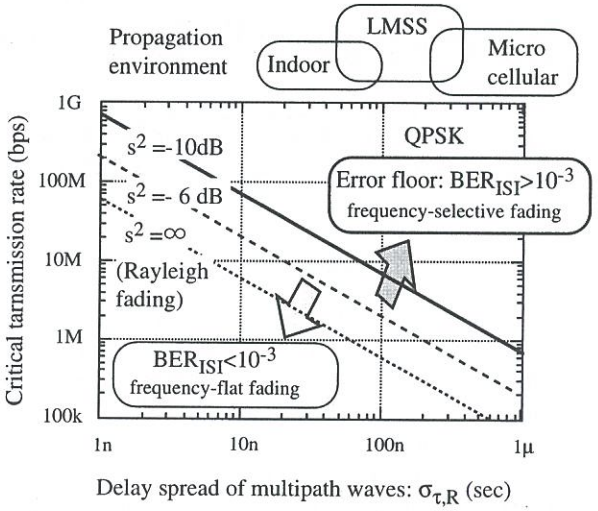

Figure 14. The critical transmission bit rate for various propagation environments.

In Figure 13, the solid lines show the calculated BER_{ISI} as a function of s^2, when $\sigma_{\tau,R}=\tau_m=0.05T_s$, $0.1T_s$, $0.2T_s$, and $0.3T_s$ for CQPSK. In this figure, the results calculated using the single parameter of σ_τ in Equation (8) (that is, the equivalent Rayleigh-fading approximation) are shown by dotted lines. As for a comparison between Nakagami-Rice fading and equivalent Rayleigh fading with the same delay profile, the difference becomes very small for s^2 above 0 dB. On the other hand, in conditions with smaller values of s^2, such that $s^2 < -2$ dB, considerable differences can be seen between the two. In the Nakagami-Rice fading model shown in Figure 13 (solid line), a very accurate estimate can be expected in a line-of-sight fading environment, as well as in a Rayleigh fading environment.

It can be concluded that the ETP model is a simple, accurate, and powerful tool for analyzing digital-transmission characteristics in a line-of-sight fading environment, as well as in a Rayleigh fading environment.

Finally, the critical transmission bit rate for QPSK – which is defined as the bit rate where the BER degrades by 10^{-3} – is shown in Figure 14 as a function of the delay spread ($\sigma_{\tau,R}$) and the multipath power ratio (s^2), for various propagation environments. This might be helpful when judging whether special countermeasures for wideband digital transmission – such as an equalizer, or a multi-carrier transmission scheme – are necessary.

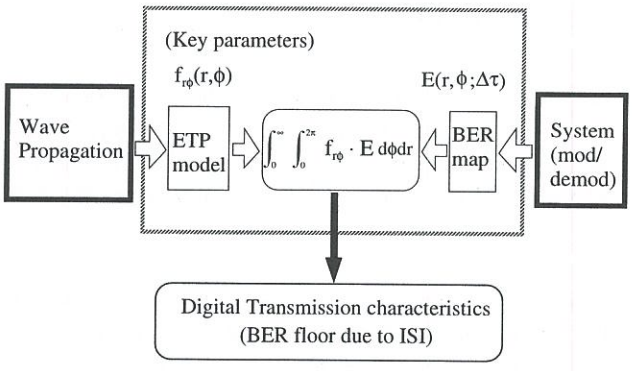

Figure 15. The relationship between "wave propagation" and "systems" in BER_{ISI} estimation.

8. Conclusion

A very simple but general scheme for calculating the irreducible bit-error rate (the BER floor), due to inter-symbol interference (ISI), in frequency-selective Nakagami-Rice fading environments has been reviewed. The scheme, which we call the equivalent transmission-path model (ETP model), connects wave propagation with digital transmission characteristics in a general manner. The role of this model is summarized in Figure 15.

In this paper, after reconfiguring our papers on the ETP model, we presented a consistent calculation formula for the BER due to ISI. In order to show application examples, we analyzed wideband digital transmission characteristics in terms of averaged BER and EOR (specifically, the percentage of locations where the BER exceeds a threshold value), in the case of an indoor propagation environment. The ETP model is expected to be a powerful tool for the analysis of OFDM (orthogonal frequency-division multiplexing) transmission characteristics, where the delay spreading exceeds the guard interval. We will carry out this analysis in the next step.

9. References

1. Y. Karasawa, T. Kuroda, and H. Iwai, "The Equivalent Transmission-Path Model – A Tool for Analyzing Error Floor Characteristics due to Intersymbol Interference in Nakagami-Rice Fading Environments," *IEEE Transactions on Vehicular Technology*, **VH-46**, 1, 1997, pp. 194-202.
2. H. Iwai and Y. Karasawa, "The Theoretical Foundation and Applications of Equivalent Transmission-Path Model for Assessing Wideband Digital Transmission Characteristics in Nakagami-Rice Fading Environments," *IEICE Trans. Communications*, **E79-B**, 9, 1996, pp. 1205-1214.
3. Y. Karasawa and H. Iwai, "Enhancement of the ETP Model: How to Calculate BER due to ISI for Wideband Digital Transmission in Nakagami-Rice Fading Environments," *IEEE Transactions on Vehicular Technology*, **VH-49**, 6, 2000, pp. 2113-2120.

Continued on page 26

Continuation from page 15

4. Y. Karasawa, T. Kuroda, and H. Iwai, "Analysis of Cycle Slip in Clock Recovery on Frequency-Selective Nakagami-Rice Fading Channels based on the Equivalent Transmission-Path Model," *IEICE Trans. Commun.*, **E79-B**, 12, 1996, pp. 1900-1910.
5. P. A. Bello and B. D. Nelin, "Effect of Frequency Selective Fading on the Binary Error Probability of Incoherent and Differentially Coherent Matched Filter Receiver," *IEEE Transactions on Communications Systems*, **CS-11**, 1963, pp. 170-186.
6. P.A. Bello, "Characterization of Randomly Time-Variant Linear Channels," *IEEE Transactions on Communication Systems*, **CS-11**, 1963, pp. 360-393.
7. D. Parsons, *The Mobile Radio Propagation Channel*, London, Pentech Press, 1992.
8. S. Y. Seidel and T. S. Rappaport, "Site-Specific Propagation Prediction for Wireless In-Building Personal Communication System Design," *IEEE Transactions on Vehicular Technology*, **VH**-43, 4, 1994, pp. 879-891.
9. R. A. Valenzuela, "A Ray Tracing Approach in Predicting Indoor Wireless Transmission," in *Proceedings of the IEEE 43rd Vehicular Technology Conference*, May 1993, pp. 214-218.
10. J. W. McKown and R. L. Hamilton, "Ray Tracing as a Design Tool for Radio Networks," *IEEE Network Magazine*, November 1991, pp. 27-30.
11. T. Manabe, Y. Miura, and T. Ihara, "Effects of Antenna Diversity and Polarization on Indoor Multipath Propagation Characteristics at 60 GHz," *IEEE Journal on Selected Areas of Communications*, **14**, 3, 1996, pp. 441-447.
12. N. Gejoh and Y. Karasawa, "A Simple Calculation Method on Spatial Distribution of Errors due to ISI Based on the ETP Model; Application to an Indoor Propagation Environment," IEICE Report of Technical Group on Antennas and Propagation, No. A.P2000-200, February 2001, pp. 33-40 (a paper with the same content is now under review by *IEICE Trans. Comm.*).
13. K. Sato et al., "Measurement of Reflection and Transmission Characteristics of Interior Structures of Office Building in the 60-GHz Band," *IEEE Transactions on Antennas and Propagation*, **AP-45**, 12, 1997, pp. 1783-1792.